1 **Frontotemporal dementia mutant tau (P301L) locks Fyn in an open, active conformation**

2 **conducive to nanoclustering**

3

4 Christopher Small[1,#], Ramón Martínez-Mármol[1,#,*], Tristan P. Wallis[1], Rachel S. Gormal[1],

5 Jürgen Götz[1,*] and Frédéric A. Meunier[1,*]

6

7 [1]Clem Jones Centre for Ageing Dementia Research (CJCADR), Queensland Brain Institute

8 (QBI), The University of Queensland, St Lucia Campus, Brisbane, QLD 4072, Australia

9

10 [#]These authors contributed equally.

11

12

13 [*]Senior corresponding authors: Frédéric A. Meunier (f.meunier@uq.edu.au), Ramón Martínez-

14 Mármol (r.martinezmarmol@uq.edu.au) and Jürgen Götz (j.goetz@uq.edu.au)

Abstract

Fyn is a Src kinase that controls critical signalling cascades and its postsynaptic enrichment underpins synaptotoxicity in Alzheimer's disease (AD) and frontotemporal dementia (FTLD-tau). Previously, we found that pathogenic FTLD tau mutant (P301L) expression promotes aberrant trapping of Fyn in nanoclusters within hippocampal dendrites via an unknown mechanism (Padmanabhan et al., 2019). Here, we imaged Fyn-mEos2 using single particle tracking photoactivated localization microscopy (sptPALM) to demonstrate that nanoclustering of Fyn in hippocampal dendrites is promoted by Fyn's open, primed conformation. Disrupting the auto-inhibitory, closed conformation of Fyn through phospho-inhibition, and perturbation of Fyn's SH3 domain increases, Fyn's nanoscale trapping. However, inhibition of Fyn's catalytic domain has no impact on its mobility. Tau-P301L promotes Fyn lateral trapping via Fyn opening and ensuing increased catalytic activation. Pathogenic tau may therefore drive synaptotoxicity by locking Fyn in an open, catalytically active conformation, leading to postsynaptic entrapment and aberrant signalling cascades.

Introduction

Fyn is a member of the Src family of kinases (SFKs), a group of enzymes that regulate signal transduction by catalysing the phosphorylation of tyrosine residues. Fyn is expressed in numerous cell-types, including lymphocytes, neurons and glia, and like other SFKs, is an intracellular, membrane-associated enzyme characterised by four conserved motifs known as Src homology domains (SH1, SH2, SH3 and SH4) (Figure 1A i). The SH1 domain is the catalytic domain responsible for the phosphorylation of tyrosine residues from target proteins and is connected via a polyproline type II (PPII) helix linker region to the SH2 domain (Figure 1A ii-iii). The SH2 and SH3 domains control the interaction of Fyn with its substrates, and the N-terminal SH4 domain is responsible for the association with the plasma membrane through myristylation and palmitoylation, thereby facilitating the interaction between Fyn and its membrane-associated substrates (Sato et al., 2009). The kinase activity of Fyn is also controlled by the transition between a closed (assembled) (Figure 1A ii) and an open (extended) conformation that can bind to its substrates and execute its catalytic activity (Figure 1Aiii). This transition is controlled by two conserved tyrosine phosphorylation sites with opposing roles. Dephosphorylation of Y531 in the C-terminal tail opens Fyn, resulting in its priming. This extended-primed form of Fyn is activated by trans-autophosphorylation of Y420, located in a central "activation loop" of the SH1 catalytic domain (Young et al., 2001). In the open conformation, the SH2 and SH3 domains are displaced and are free to interact with external ligands (Yadav & Miller, 2007). Conversely, two intramolecular interactions with the SH2 and SH3 domains are essential for downregulation of the kinase activity (Engen et al., 2008; Huculeci et al., 2016). Phosphorylation of Y531 allows this residue to interact with the SH2 domain and stabilises an assembled conformation whereby kinase activity is decreased by conformational changes at the active site of the catalytic domain. The second downregulatory interaction includes the SH3 domain and the PPII helix linker. Interestingly, this intramolecular

57 interaction resembles the standard binding mode of SH3 domains to target sequences rich in

58 proline and other hydrophobic amino acids (P-X-X-P motif, where P is proline and X is any

59 amino acid). These sequences generally form a PPII helix which associates with the

60 hydrophobic surface of the SH3 domain (Engen et al., 2008).

61

62 Fyn is responsible for integrating multiple signalling cascades. In neurons, Fyn facilitates cell-

63 to-cell communication by promoting the scaffolding of the N-methyl-D-aspartate (NMDA)

64 receptor through phosphorylation of the NR2B subunit of the receptor at the Y1472 epitope.

65 This increases the affinity of NR2B with postsynaptic density protein 95 (PSD95) and, as a

66 consequence, facilitates the stabilisation of NMDA receptor clusters at the membrane, thereby

67 maintaining postsynaptic excitatory currents (Tezuka et al., 1999). Fyn is also implicated in

68 mediating neurodegeneration. Overactive Fyn is believed to exacerbate cell death by promoting

69 excess activation of NMDA receptors, leading to aberrant calcium entry into the postsynapse

70 and neuronal excitotoxicity (Xia & Gotz, 2014). Fyn has also been shown to play a critical role

71 in the neurotoxicity of Alzheimer's disease (AD) and frontal temporal lobar degeneration with

72 tau (FTLD-tau) (Briner et al., 2020; Polanco et al., 2018). Fyn promotes neurotoxicity

73 downstream of the amyloid-beta (Aβ) peptide, which forms extracellular amyloid plaques, and

74 the microtubule-associated protein tau (MAPT). Hyperphosphorylated tau accumulates into

75 neurofibrillary tangles (NFTs), a key hallmark of the toxicity associated with AD and FTLD-

76 tau (Gotz et al., 2001). In transgenic mouse lines that replicate AD pathology, knockout of Fyn

77 has been shown to protect against the loss of presynaptic terminals and to delay premature

78 mortality (Chin et al., 2004). Hippocampal slices from Fyn knockout mice have been shown to

79 resist the toxic effects of treatment with toxic Aβ oligomers (Um et al., 2012). Similarly,

80 pharmacological inhibition of Fyn rescues the behavioural deficits observed in AD mice

81   (Kaufman et al., 2015). Conversely, overexpression of Fyn exacerbated the neuronal deficits

82   present in AD mice (Chin et al., 2005; Kaufman et al., 2015).

83

84   Increasing evidence suggests that Fyn works as a key partner in tau-mediated pathology. Fyn

85   interacts with tau through its SH2 and SH3 domains and P-X-X-P motifs located in the proline-

86   rich region of tau (Bhaskar et al., 2005; Lau et al., 2016; Lee et al., 1998). This interaction

87   mediates phosphorylation of tau at residue Y18, one of the epitopes associated with the

88   formation of NFTs in AD patients (Bhaskar et al., 2010; Lee et al., 2004; Miyamoto et al.,

89   2017; Neddens et al., 2018), and potentiates its association with Fyn (Usardi et al., 2011).

90   Subcellular compartmentalisation of Fyn and tau also appears to be crucial for their toxicity.

91   Mis-localisation of tau into dendritic spines mediates the synaptic dysfunction associated with

92   AD and FTLD-tau (Frandemiche et al., 2014; Hoover et al., 2010; Miller et al., 2014; Xia et

93   al., 2015). Fyn regulates the phosphorylation and dendritic distribution of tau through its

94   activation by Aβ during AD (Larson et al., 2012). Alternatively, a previous study found that

95   tau itself controls the localisation of Fyn to dendrites, and that disruption of postsynaptic

96   targeting of Fyn mitigates Aβ toxicity (Ittner et al., 2010).

97

98   Altered organisation of receptors and signalling molecules in nanodomains is emerging as a

99   key regulator of neuronal toxicity (Shrivastava et al., 2017). Several proteins involved in AD

100   show aberrant clustering associated with the pathology. The metabotropic glutamate receptor

101   mGluR5, for example, shows increased clustering when binding to Aβ (Renner et al., 2010);

102   and the amyloid precursor protein (APP) organises into regulatory nanodomains that control

103   the availability of APP molecules for proteolytic processing (Kedia et al., 2020). In this respect,

104   tau has been shown to control the lateral trapping of Fyn into nanodomains within the dendrites

105   and spines of hippocampal neurons, with single molecule imaging of Fyn-mEos2 showing

5

106   enhanced mobility and decreased clustering in tau knockout neurons. Importantly, expression

107   of an FTLD tau mutant (P301L) aberrantly increases the number of Fyn nanoclusters in spines,

108   an effect that is likely to contribute to NMDA-mediated excitotoxicity (Padmanabhan et al.,

109   2019). However, whether the nanoscale spatiotemporal organisation of Fyn is involved in its

110   efficient transactivation remained to be established, and the mechanisms underlying the Fyn-

111   tau toxic partnership have not yet been fully elucidated.

112

113   In this study, we used single-particle tracking photoactivated localization microscopy

114   (sptPALM) to determine how the nanoscale organisation of Fyn is affected by its activity and

115   conformation in the dendrites of live hippocampal neurons. Through pharmacological

116   inhibition, blocking phosphorylation of the Y420 residue, preventing binding of ATP to the

117   K299 epitope, or introducing a phosphorylation-inhibitory mutant to render Fyn constitutively

118   open, we evaluated whether preventing the catalytic activity or altering the overall

119   conformation can modulate Fyn mobility dynamics in neurons. Our results demonstrate that

120   the SH3 domain is essential for maintaining a closed conformation and interacting with Fyn-

121   binding proteins such as the FTLD-associated P301L mutant tau. Fyn entry into an opened,

122   primed conformation is associated with its nanoscale entrapment. This extended and confined

123   molecular configuration is compatible with the binding of pathological mutant tau to Fyn.

124   Taken together, our findings suggest a molecular mechanism in which binding of P301L tau to

125   Fyn in the dendritic compartment exacerbates Fyn's toxic effects in FTLD-tau.

126

127 **Results**

128

129 **The catalytic activity of Fyn does not alter the nanoscale organisation of Fyn in**

130 **hippocampal dendrites**

131 We recently discovered that Fyn displays a nanocluster organisation in the dendritic spines of

132 hippocampal neurons that is dynamically regulated by neuronal maturation (Padmanabhan et

133 al., 2019). In this study, we investigate whether changes in Fyn activity affect the nanoscale

134 organisation of Fyn in live neurons. Fyn-mEos2 was expressed in hippocampal neurons,

135 together with mCardinal or GFP as a cytoplasmic marker, and we performed sptPALM in an

136 oblique illumination configuration. We imaged mature neurons at DIV19-22 and selected

137 secondary dendrites with mature spines for analysis (Figure 1B). Fyn-mEos2 molecules were

138 randomly photoconverted from a green- to a red-emitting state in response to constant weak

139 illumination at 405 nm at a low spatial density. The photoconverted molecules were tracked in

140 the red-emitting channel at 561 nm excitation at 50 Hz for a duration of 320 s (16,000 frames),

141 in order to resolve the nanoscale distribution and dynamics of Fyn at a high spatiotemporal

142 resolution in live neurons (Figure 1C).

143

144 Given that Fyn has a critical role in integrating a multitude of signalling pathways in neurons

145 (Li & Gotz, 2017), we first sought to determine whether its catalytic activity was involved in

146 promoting its nanoclustering at the post-synapse. Based on experiments performed with other

147 SFKs, it is established that mutations of specific residues in the SH1 domain have profound

148 effects on the activity of these enzymes, without affecting their conformation (Engen et al.,

149 2008; Nika et al., 2010; Sicheri & Kuriyan, 1997). Trans-autophosphorylation of Y420 located

150 at the central "activation loop" of the catalytic domain is required for the transition from an

151 open, primed to an opened, active form able to phosphorylate its substrates (Nika et al., 2010;

7

152   Young et al., 2001). To determine if the trans-autophosphorylation of Y420 in the catalytic

153   SH1 domain controls the nanoclustering of Fyn, we introduced a phospho-inhibitory mutation

154   (Y420F) to generate a 'kinase-inactivated' Fyn enzyme (Figure 2A-B). Our results showed that

155   this mutation did not affect the mobility of Fyn in dendritic branches of hippocampal neurons

156   (Figure 2C i-ii). Similarly, no changes in the mobility of Fyn-mEos2 were observed in dendritic

157   spines (Figure 2D i-ii). To further evaluate the importance of Fyn activity, we generated a

158   'kinase-dead' Fyn by introducing the mutation K299M, designed to block interaction with

159   ATP, thereby creating an inactive enzyme unable to phosphorylate other substrates (Figure 2A)

160   (Jin et al., 2017; Twamley et al., 1992; Twamley-Stein et al., 1993). Similarly, the Fyn-K299M-

161   mEos2 mutation had no effect on the mobility compared to wild-type Fyn-mEos2 in dendrites

162   (Figure 2C i-ii) and spines (Figure 2D i-ii). Blockade of Fyn activity was also achieved by

163   incubating   neurons   with   3-(4-chlorophenyl)-1-(1,1-dimethylethyl)-1H-pyrazolo[3,4-

164   d]pyrimidin-4-amine (PP2) (10 μM, 30 minutes), a potent and specific pharmacological

165   inhibitor of SFK's kinase catalytic activity (Hanke et al., 1995; Jin et al., 2017; Tomatis et al.,

166   2013). We used the structurally related inactive analogue 1-phenyl-1H-pyrazolo[3,4-

167   d]pyrimidin-4-amine (PP3) (10 μM) as a control that does not inhibit Src family members

168   (Figure 2 – Figure 1 supplement) (Bain et al., 2003). PP2 is an ATP-competitive inhibitor that

169   interacts with the hydrophobic pocket near the ATP-binding cleft of the SH1 domain, thereby

170   preventing the binding of the substrate ATP to the enzyme (Zhu et al., 1999). No alterations in

171   Fyn-mEos2 mobility were observed in the dendrites of hippocampal neurons in response to

172   PP2 or PP3 treatment (Figure 2-Figure 1 supplement) suggesting that the catalytic activity had

173   no influence on the nanoscale organisation of Fyn at the synapse. Overall, these results further

174   support the notion that the catalytic activity of Fyn does not influence its nanoscale organisation

175   at the post-synapse.

176

177 Induction to an open, primed conformation promotes the nanoscale entrapment of Fyn

178 in hippocampal dendrites and spines

179   The closed conformation of Fyn is primarily maintained through phosphorylation of the Y531

180   epitope in the C-terminal tail, which stabilises the interaction of the C-terminal domain of Fyn

181   with its SH2 region. To constitutively force an open conformation, we introduced a phospho-

182   inhibitory mutation (Y531F) into the C-terminal domain of Fyn (Figure 3A). The opened-

183   primed conformation rapidly facilitates the trans-autophosphorylation on Y420 that results in

184   a fully active enzyme. In the presence of the Y531F mutation, Fyn is unable to return to its

185   inactive-closed conformation, resulting in a 'constitutively-active' form of Fyn (Nakazawa et

186   al., 2001; Xia & Gotz, 2014). To examine the effect of Y531F-induced constitutively open

187   conformation on the mobility of Fyn in dendrites, we performed sptPALM of Fyn-Y531F-

188   mEos2. We observed a significant decrease in Fyn mobility, indicating that the open

189   conformation of Fyn is essential for mediating the nanoscale lateral trapping of Fyn within

190   dendrites (Figure 3C i-ii) and spines (Figure 3D i-ii). To evaluate whether the kinase activity

191   of Fyn played a role in its immobilization, or whether this effect was solely associated with a

192   change in the conformation towards an extended one, we created the mutant Fyn-Y531F-

193   K299M, that remains constitutively opened but with an inactive catalytic domain (Figure 3A).

194   This double mutant also showed significantly lower mobility than the wild-type Fyn in

195   dendrites (Figure 3C i-ii) and spines (Figure 3D i-ii). Interestingly, our results revealed an

196   attenuation of the opened Fyn immobilization in the presence of the K299M mutation (Figure

197   3C-D). This observation suggests that modifying the catalytic domain through the K299M

198   mutation somehow interferes with Fyn's open conformation. In summary, these results

199   demonstrate that the nanoscale organisation of Fyn is principally controlled by its entry into an

200   open, primed conformation through dephosphorylation of the Y531 epitope.

201

202   To determine if the changes in mobility observed with the Y531F mutant were a product of an

203   alteration in the lateral trapping of Fyn-mEos2 molecules, we compared the frequency

204   distribution (%) of inter-frame step lengths taken by Fyn-WT-mEos2 and Fyn-Y531F-mEos2

205   throughout our acquisitions. Interestingly, the average inter-frame step size of Fyn-WT-mEos2

206   throughout its lifespan was not significantly different from that of the Y531F mutant (Figure

207   4A), suggesting that the changes in mobility of the Y531F mutant may be due a perturbation

208   in the nanoclustering of Fyn-mEos2. To investigate this, we used Density-Based Spatial

209   Clustering of Applications with Noise (DBSCAN) to quantify the size and density of Fyn-

210   mEos2 nanoclusters (Figure 4B-D). This approach involved evaluating the spatial distribution

211   of Fyn-mEos2 trajectory centroids, which allowed us to determine which of those trajectories

212   were confined within spatial clusters, and to derive metrics on cluster number, area, density

213   and trajectory mobility. DBSCAN analysis confirmed that wild-type Fyn had decreased

214   mobility when organised in small nanoclusters at the synapse (Figure 4B) that occupy an

215   average area of 0.271 ± 0.016 μm^2. Within these nanoclusters, the mobility and displacement

216   of Fyn were restricted (Figure 4C i). The Y531F mutation, which induces an active, open

217   conformation, caused Fyn-mEos2 to have a significantly lower mobility (MSD) within

218   nanoclusters (Figure 4C ii). Furthermore, the Y531F mutation caused Fyn-mEos2 to be

219   packaged into smaller nanoclusters (0.124 ± 0.006 μm^2) with increased trajectory membership

220   (Figure 4D i) and of significantly higher density (Figure 4D ii-iii). These results led us to

221   conclude that the decreased mobility of Fyn-mEos2 observed in its open conformation was due

222   to increased nanoclustering propensity, rather than a decrease in the size of the inter-frame

223   steps of Fyn-mEos2 molecules.

224

225   **Alteration of the SH3 domain renders Fyn more immobile in dendrites**

226 The intramolecular interaction between the SH3 domain and the PPII helix linker is also

227 essential to stabilise the inactive, closed conformation of Fyn and other SFKs (Moroco et al.,

228 2014; Young et al., 2001). As a consequence, displacement of the SH3 domain from the helix

229 linker has been reported to facilitate the activation of these kinases (Briggs & Smithgall, 1999;

230 Moroco et al., 2014). The SH3 domain is also involved in the interaction of Fyn with its

231 substrates such as the heterogeneous nuclear ribonucleoprotein A2 (hnRNPA2) (Amaya et al.,

232 2018), p85α (Morton et al., 1996), the palmitoyl-acyl transferase DHHC5 (Brigidi et al., 2015),

233 tau (Lee et al., 1998; Reynolds et al., 2008) and P301L mutant tau (Bhaskar et al., 2005). As

234 displacement of the SH3 domain has been used to activate Fyn molecules and other SFKs

235 (Moroco et al., 2014), we wanted to explore whether direct alterations of this domain affects

236 the nanoscale organisation of Fyn. To investigate this, we performed sptPALM on a Fyn

237 protein lacking the SH3 domain (Fyn-ΔSH3-mEos2) (Figure 5A, B). Deletion of the SH3

238 domain resulted in a decreased mobility of Fyn (Figure 5C, D). In accordance to what has been

239 observed through alteration of the SH3 domain in other SFKs (Moroco et al., 2014), our results

240 may suggest that the absence of the SH3 domain destabilises the closed conformation of Fyn.

241 Similar to the Y531F mutation, this could facilitate the transition of Fyn to the open, primed

242 conformation, leading to Fyn's immobilisation.

243

244 Due to the importance of the SH3:helix linker interaction in stabilising the closed conformation

245 of SFKs, several strategies have been developed to manipulate the activity of these enzymes

246 based on the creation of small molecules that selectively bind the SH3 domain (Huang et al.,

247 2016; Kukenshoner et al., 2017; Moroco et al., 2014; Yadav & Miller, 2007). The G9

248 monobody was specifically generated to interact with the SH3 domain, displaying high

249 specificity for Fyn among other kinases (Huang et al., 2012). To further evaluate how

250 alterations of the SH3-PPII helix linker interaction affects the nanoscale organisation of Fyn,

251 we created a mEos2 tagged version of the G9 monobody (Figure 6A). As a control, we used a

252 mEos2-tagged anti-GFP nanobody co-transfected with Fyn-GFP in HEK293 cells (Figure 6A,

253 B). Our results demonstrate that the anti-GFP-mEos2 nanobody, co-expressed with Fyn-GFP,

254 displays similar mobility to Fyn-mEos2 alone. However, co-expression of Fyn-GFP together

255 with the mEos2 G9 anti-Fyn-mEos2 monobodies targeting the SH3 domain, resulted in a

256 significant decrease in the MSD of Fyn-GFP in HEK293T cells (Figure 6C). This result

257 suggests that binding of monobodies to the SH3 domain of Fyn causes an increase in the

258 immobilisation of Fyn molecules. Interfering with the SH3-PPII helix linker region may

259 therefore facilitate the acquisition of a conformation conducive to lateral trapping of extended-

260 primed Fyn molecules.

261

262 **Overexpression of wild-type and FTLD-tau mutant (P301L) tau promotes an open**

263 **conformation and immobilisation of Fyn in hippocampal dendrites**

264 Previous findings suggest that aberrant nanoclustering is enhanced by the presence of a FTLD

265 mutant form of tau (P301L) (Padmanabhan et al., 2019). This mutant tau binds to the SH3

266 domain of Fyn with higher affinity than wild-type tau (Bhaskar et al., 2005). To further evaluate

267 the effect of wild-type and P301L mutant tau on the mobility of Fyn-mEos2, we co-expressed

268 wild-type tau and P301L mutant tau with Fyn-mEos2 in hippocampal neurons and performed

269 sptPALM imaging (Figure 7A). Wild-type tau caused a significant decrease in the mobility of

270 Fyn-mEos2 (Figure 7B, C). In accordance with our previous findings, this decrease was

271 accentuated in the presence of P301L tau (Figure 7B, C), which has an increased binding

272 capacity to Fyn (Bhaskar et al., 2005). This is interesting as tau binds Fyn through its SH3

273 domain, which causes a decrease in Fyn mobility when disrupted. These results suggest that

274 the intramolecular interaction between the SH3 and PPII helix linkers regions plays a key role

275 in controlling the nanoscale organisation of Fyn, and that wild-type and P301L mutant tau

12

276   drives the nanoclustering of Fyn by displacing this interaction and thus stabilising an open and

277   highly immobile Fyn conformation. We co-expressed Fyn and tau or tau-P301L in HEK293T

278   cells and observed that the total expression of Fyn increased in the presence of P301L mutant

279   tau, and that the proportion of phosphorylated Fyn (Y420) was also higher (Figure 7D). Taken

280   together, these findings suggest that the interaction of Fyn with P301L tau exposes and primes

281   the Y420 epitope for phosphorylation, a process which is associated with increased

282   nanoclustering in hippocampal neurons.

283

Discussion

285   Fyn is an SFK whose activity integrates multiple signalling cascades. However, when

286   dysregulated, Fyn has been associated with the development of neurological disorders such as

287   AD and tau pathologies (Haass & Mandelkow, 2010; Ittner & Gotz, 2011). We recently

288   provided the first conceptual framework for how the nanoscale organisation of Fyn is altered

289   during tau-mediated neurodegeneration (Padmanabhan et al., 2019). However, it is not known

290   whether the nanoscale spatiotemporal organization of Fyn is required for its efficient signal

291   transduction, and the mechanisms driving the toxic partnership of Fyn and tau remains

292   unsolved. Our new results now suggest that the transition of Fyn into an open conformation

293   facilitates its organization into nanoclusters, and that the binding of toxic P301L mutant tau

294   associated with FTLD-tau locks Fyn into an open, immobile and catalytically active

295   conformation, thereby providing a rational explanation for the resulting initiation of aberrant

296   toxic signalling cascades.

297

298   The kinase activity of Fyn and other SFKs is controlled by the transition between two opposing

299   configurations (from closed/inactive to open/primed). This transition allows SFKs to bind their

300   substrates and execute their catalytic activity (Sicheri & Kuriyan, 1997). Closed Fyn is locked

301   through two intramolecular interactions between the SH2 domain bound to phosphorylated

302   Y531 at the C-terminal tail, and the interaction between the hydrophobic residues from the

303   SH3 domain with the proline-rich PPII helix linker (Engen et al., 2008). Our results showed

304   that altering any of the locking interactions reduces the mobility of Fyn, suggesting that its

305   transition into an open, primed conformation promotes its lateral entrapment. Opening of SFKs

306   triggers their catalytic activity because the SH2 and SH3 domains become accessible to interact

307   with external ligands (Yadav & Miller, 2007), and the SH1 catalytic domain can be activated

308   immediately after trans-autophosphorylation of Y420 (Young et al., 2001). In contrast, we

309   found that the catalytic activity of the SH1 domain has little impact on the mobility of Fyn.

310   This finding was demonstrated by the observations that (1) neither genetic or pharmacological

311   suppression of Fyn activity had an impact on Fyn mobility, and (2) creation of an open-but-

312   inactive Fyn through addition of the "kinase-dead" K299M mutant on top of the "open" Y531F

313   mutant had little effect on Fyn immobilisation. Taken together, our findings indicate that the

314   nanoscale organisation of Fyn is only affected by changes in its conformation, and that

315   acquisition of an open, extended structure induces its lateral trapping in dendritic nanoclusters.

316   In addition, as conformation and activity changes are interdependent in SFK enzymes, it is

317   likely that the nanoclustering of Fyn facilitates its catalytic activity, being required to initiate

318   its downstream signalling at the post-synapse.

319

320   The fact that SFKs are broadly expressed and share a common negative regulatory mechanism

321   based on intramolecular interactions involving the SH2:tail and SH3:linker has motivated

322   extensive research in exploiting these properties, to design strategies based on the creation of

323   synthetic SH2/SH3-binding small molecules to finely control the activity of SFKs (Huang et

324   al., 2016; Kukenshoner et al., 2017; Moroco et al., 2014; Yadav & Miller, 2007). Interestingly,

325   monobodies (Huang et al., 2016; Huang et al., 2012) and peptoid-based ligands (Li &

326   Lawrence, 2005) that are highly selective for the Fyn SH3 domain have already been generated

327   to modulate the activity of Fyn kinase. We used a mEos2-tagged version of the G9 monobody

328   created specifically to selectively bind Fyn SH3 domain (Huang et al., 2012). As Fyn interacts

329   with tau through its SH2 and SH3 domains (Bhaskar et al., 2005; Lau et al., 2016; Lee et al.,

330   1998), it is conceivable that binding of our G9-mEos2 monobody to the SH3 domain could

331   induce a steric effect that interferes with the conformational mobility of Fyn in a similar way

332   to tau. Our results indicate that binding of the G9-mEos2 monobody reduces the mobility of

333   Fyn molecules, reinforcing the idea that alteration of their closed state by interfering with the

334   intramolecular SH3:linker promotes an open-primed and immobilised Fyn conformation. The

335   equilibrium dissociation constant (K_D) for G9 monobodies bound to the Fyn SH3 domain

336   calculated using isothermal titration calorimetry is 0.166 μM (Huang et al., 2012). In a different

337   study using surface plasmon resonance, the K_D values calculated for WT tau and tau P301L

338   bound to the SH3 domain of Fyn were 6.77 μM and 0.16 μM, respectively (Bhaskar et al.,

339   2005). Although different techniques were used, these results suggest that G9 monobodies bind

340   to the SH3 domain of Fyn with higher affinity than tau, and at comparable level as the FTLD

341   mutant tau. These results are in line with our observations where overexpression of the mutant

342   P301L tau decreased Fyn mobility to a similar extent as G9 monobodies do.

343

344   Interaction between tau and Fyn contribute to neurodegeneration associated with AD (Ittner et

345   al., 2010) and FTLD-tau (Liu et al., 2020; Tang et al., 2020). Manipulating this interaction has

346   been suggested as a potential therapeutical intervention. Decreasing either tau (Rapoport et al.,

347   2002) or Fyn (Lambert et al., 1998; Um et al., 2012), for example, protects against Aβ toxicity

348   in AD. However, undesired effects such as memory deficits associated with the absence of Fyn

349   (Grant et al., 1992) suggest that further investigations are required to achieve more desirable

350   therapeutic results. The recent development of a cell-permeable peptide inhibitor of the Fyn-

15

351 tau interaction yielded promising results, reducing the endogenous Fyn-tau interaction and tau

352 phosphorylation (Rush et al., 2020). G9 monobodies have also been used, demonstrating

353 efficiency in inhibiting Fyn-tau binding (Cochran et al., 2014). Our findings on Fyn mobility

354 using G9 monobodies against the SH3 domain are in line with these results and add the analysis

355 of nanoscale mobility using super-resolution microscopy as a powerful new tool to evaluate

356 potential therapeutical candidates.

357

358 Nanoclustering has been linked to the increased activity of multiple pre- and postsynaptic

359 molecules, including AMPA receptors (Nair et al., 2013), syntaxin1A (Bademosi et al., 2017)

360 and Munc18-1 (Chai et al., 2016). In particular, nanoclustering of syntaxin1A, which is

361 associated with increased exocytosis, is driven by analogous mechanisms to those observed for

362 Fyn. Syntaxin1A, a soluble N-ethylmaleimide-sensitive factor attachment protein receptor

363 (SNARE) that drives vesicle fusion at the presynapse, switches from an inactive, closed

364 conformation to an open conformation that can bind other SNARE proteins to initiate the fusion

365 of synaptic vesicles with the plasma membrane. Interaction with the chaperone Munc18-1

366 promotes the folding of syntaxin1A into a closed and inactive state. Detachment of Munc18-1

367 facilitates the entry into an open conformation that allows syntaxin1A to interact with other

368 SNARE proteins and form nanoclusters, thereby driving exocytosis at the presynapse (Kasula

369 et al., 2016; Padmanabhan et al., 2020). Similarly, Fyn molecules fluctuate between a closed

370 and an open conformation, the latter being enzymatically active and more immobile, and tau

371 working as a molecular chaperone that modulates this transition.

372

373 We have previously reported that Fyn is organised in compacted nanodomains in dendrites

374 (Padmanabhan et al., 2019), suggesting molecular crowding (Goose & Sansom, 2013; Li et al.,

375 2016), spine geometry (Byrne et al., 2011) and interaction with neighbouring proteins as

16

376   mechanisms that regulate the trapping and nanodomain organization of Fyn. Extension of Fyn

377   molecules exposes their SH2 and SH3 motifs (Huculeci et al., 2016), and our results indicate

378   that opening this conformation induces lateral trapping of Fyn into nanoclusters. However, it

379   is unclear which interactions are responsible for this effect. Self-association has been described

380   for other SFKs, with the formation of dimers enabling rapid potentiation of their activity when

381   the enzymes adopt an open conformation (Irtegun et al., 2013). This suggests that

382   multimerisation of opened, primed Fyn molecules could facilitate their clustering in dendrites.

383   PSD95 is another possible candidate, as it stabilises molecules at the post-synapse and forms

384   spine nanodomains of comparable size and frequency to those of Fyn (Hruska et al., 2018; Nair

385   et al., 2013). Both PSD95 and Fyn associate with the plasma membrane following

386   palmitoylation of specific residues (Sato et al., 2009; Tezuka et al., 1999; Topinka & Bredt,

387   1998) and PSD95 interacts with the SH2 domain of Fyn (Tezuka et al., 1999). This suggests

388   that entry into an open conformation may induce Fyn to bind to PSD95, resulting in their

389   postsynaptic nanoclustering. Tau also interacts with Fyn, and has previously been shown to

390   control its localisation and nanoclustering in dendrites (Ittner et al., 2010; Padmanabhan et al.,

391   2019). However, it is unclear whether this effect reflects a direct interaction with tau or is

392   caused by tau's regulation of the cytoskeleton in neurons. In this respect, tau interacts with

393   actin (Cabrales Fontela et al., 2017; Elie et al., 2015) and the P301L mutant tau induces aberrant

394   presynaptic actin polymerisation that is capable of crosslinking synaptic vesicles and restricting

395   their mobilisation (Zhou et al., 2017). The actin cytoskeleton modulates nanoclustering of

396   membrane proteins (Torreno-Pina et al., 2016), opening the possibility that it could also

397   modulate the nanoscale organisation of Fyn. Further work is therefore needed to evaluate the

398   potential involvement of the actin cytoskeleton in Fyn nanoclustering. Analysis of the kinetic

399   parameters of the interaction between the SH3 domain of Fyn and pseudo-phosphorylated

400   forms of tau and mutant forms associated with FTLD-tau, showed increased binding affinities

17

401   when compared to wild-type tau, with the FTLD-tau mutant variant P301L having the highest

402   SH3 affinity (Bhaskar et al., 2005). The interaction between Fyn and tau has been extensively

403   characterised in terms of the residues responsible for this binding (Bhaskar et al., 2005;

404   Cochran et al., 2014; Lau et al., 2016; Lee et al., 1998; Usardi et al., 2011; Wang et al., 2019)

405   and the amino acids that are phosphorylated as a consequence (Lee et al., 2004). However, the

406   crystal structure that would provide a detailed representation of how Fyn and tau interact is still

407   missing. Although we lack precise structural information of Fyn-tau binding, it is therefore

408   tempting to speculate that P301L tau may stabilize an open conformation, thereby promoting

409   nanoclustering of Fyn at the post-synapse (Figure 8). Unfortunately, our temporal and spatial

410   resolution limits do not allow us to determine whether the P301L mutant tau preferentially

411   interacts with Fyn in its open state, or the binding of the mutant tau induces a conformational

412   change that extends the structure of Fyn. Although it is possible that the nanoclustering of Fyn

413   is facilitated by other interactions, our previous results suggest that P301L tau preferentially

414   drives the cluster state of Fyn in hippocampal dendrites (Padmanabhan et al., 2019). Our new

415   findings reveal the formation of a more immobile and active form of Fyn through interaction

416   with P301L mutant tau, when compared to wild-type tau. Interestingly, in a FTLD-tau

417   transgenic mice model, the loss of dendritic spines associated with impairment of spine

418   plasticity occurs in the absence of detected hyperphosphorylated tau species or NFTs

419   (Hoffmann et al., 2013). These findings are in line with observations from brain tissue of AD

420   patients (Blazquez-Llorca et al., 2011; Merino-Serrais et al., 2013). Prefibrillar tau species such

421   as tau monomers, dimers and higher order oligomeric aggregates are responsible for the

422   neurotoxic effects in AD (Polanco et al., 2018), and have been suggested as a cause for the

423   impairment in spine plasticity. However, our findings further suggest the neurotoxicity from

424   P301L tau-mediated Fyn over-activity as a plausible complementary new mechanism

425   responsible for the early loss in spine plasticity and morphology defects. Overall, the results

426 presented in here support the idea that the ability of the tau to associate with Fyn is increased

427 in FTLD-tau, altering the nanoscale organisation of Fyn and promoting an aberrant over-

428 activity that potentiates neurodegeneration.

429
430

Experimental procedures

Animal ethics and mouse strains

All experimental procedures were conducted under the guidelines of the Australian Code of Practice for the Care and Use of Animals for Scientific purposes and were approved by the University of Queensland Animal Ethics Committee (QBI/254/16/NHMRC). Wild-type mice (C57Bl/6 strain) used throughout the study were maintained on a 12-h light/dark cycle and housed in a PC2 facility with *ad libitum* access to food and water.

Primary hippocampal cultures

Primary hippocampal neurons were prepared as described previously (Joensuu et al., 2017; Padmanabhan et al., 2019). Briefly, pregnant dams (C57Bl/6 mice) were euthanised using cervical dislocation, from which embryos (E16) were extracted and dissected in 1x Hank's buffered salt solution (HBSS), 10 mM HEPES pH 7.3, 100 U/ml penicillin-100 µg/ml streptomycin (GIBCO-Thermo Fisher Scientific). Subsequently, the dissected hippocampal tissue was digested with trypsin (0.25% for 10 minutes). Digestion was halted by addition of Fetal Bovine Serum (FBS) (5%) (GIBCO-Thermo Fisher Scientific) with DNase I (Sigma) to prevent tissue clumping. The digested hippocampal tissue was left to incubate (37°C for 10 minutes). Following this, the hippocampal tissue was triturated and centrifuged (120 g, 7 min) and resuspended in neurobasal media, 100 U/ml penicillin-100 µg/ml streptomycin, 1x GlutaMAX supplement (GIBCO-Thermo Fisher Scientific), 1x B27 (GIBCO-Thermo Fisher Scientific) and Foetal Bovine Serum (FBS) (5%) (GIBCO-Thermo Fisher Scientific). Neurons were seeded in Poly-L-Lysine coated 29 mm glass-bottom dishes (Cellvis, CA, USA) at a density of 0.8-1 x10^5 neurons. A full media change was performed 2 hours after seeding using culturing media (Neurobasal Medium, 100 U/ml penicillin-100 µg/ml streptomycin, 1x GlutaMAX supplement, 1x B27).

456

Heterologous cell cultures

457

458   HEK-293T cells were maintained in DMEM media (GIBCO-Thermo Fisher Scientific)

459   supplemented with FBS (10%), 1x GlutaMAX and 100 U/ml penicillin-100 μg/ml

460   streptomycin. Cells were transfected using the Lipofectamine™ LTX reagent according to the

461   manufacturer's instructions (Invitrogen-Thermo Fisher Scientific).

462

463   **Plasmids and reagents**

464   The plasmid that codes for an FN3 monobody targeted against Fyn SH3 domain was a generous

465   gift from Emeritus Professor Brian Kay (University of Illinois at Chicago, Illinois, US). The

466   FN3 monobody was subcloned into the mEos2-N1 plasmid (Kasula et al., 2016) by inserting

467   BamHI and EcoRI restriction sites at the N- and C-termini of the monobody, followed by

468   BamHI/EcoRI digestion and ligation into mEos2 vector. Fyn mutant constructs were generated

469   by site-directed mutagenesis, using the QuikChange II site-directed mutagenesis kit (Agilent),

470   on the mEos2 donor vector containing full-length human Fyn isoform 1 (Padmanabhan et al.,

471   2019) as a template. All the resulting plasmids were sequenced using the service of the AEGRC

472   sequencing facility (The University of Queensland). PP2 and PP3 reagents were purchased

473   from Calbiochem (Merck/Millipore).

474

475   **Western blotting**

476   HEK293T cells were seeded in a 6 well plate and co-transfected with three combinations of

477   plasmid (2 μg, 24 hrs with Opti-MEM and lipofectamine LTX with Plus Reagent): Fyn-mEos2

478   + GFP, Fyn-mEos2 + tau-GFP or Fyn-mEos2 + tau-P301L-GFP. HEK293T cells were isolated

479   following trypsin digestion. Protein homogenates were boiled at 95°C in Laemelli buffer, run

480   on a Tris-Glycine Precast Gel (4-15%, Bio-Rad) at 150V and subsequently transferred to a

481 PVDF-FL membrane (Millipore), which was incubated in blocking buffer (Odyssey, TBS) for

482 1 hour at room temperature. Subsequently, membranes were incubated with primary antibody.

483 Membranes were stained for total Fyn (1:1000 rabbit anti-Fyn, Cell Signalling Technology),

484 active Src (1:1000 rabbit anti-phosphor-Y16, Santa Cruz), GAPDH (1:1000 mouse anti-

485 GAPDH, abcam #189095) and GFP (1:1000 rabbit anti-GFP, Millipore #AB3080P); in

486 blocking buffer overnight (4°C). Membranes went through TBS-T washes (5x) and incubated

487 in secondary antibody (1:10000 donkey anti-mouse 680, Li-Cor Biosciences #32212 and

488 donkey anti-rabbit 800, Li-Cor Biosciences #68023) with in Odyssey (TBS) blocking buffer (1

489 hour at room temperature). Fyn activity was measured as a ratio of phosphorylated Y416

490 intensity to total Fyn intensity, normalised to GAPDH.

491

492 **Single-particle tracking Photo-activated Localization Microscopy (sptPALM)**

493 Neurons were transfected at DIV 14 using lipofectamine 2000 (ThermoFisher Scientific) (2 μg

494 of GFP or mCardinal with 3 μg Fyn-mEos2 for 4 hrs) and were subsequently left to incubate

495 for 24 hrs prior to imaging. Acquisitions (16 000 frames at 50Hz) were taken at 37°C on the

496 Roper Scientific TIRF microscope fitted with an ILas^2 double illuminator (Roper Scientific), a

497 CFI Apo 100x/1.49N.A. oil-immersion objective (Nikon Instruments) and an evolve 512 Delta

498 EMCCD cameras (Photometrics). A Perfect Focus System (Nikon) and an iLas2 double laser

499 illuminator (Roper Scientific) was used for 360°C TIRF illumination. MetaMorph software

500 (version 7.10.2, Molecular Devices) was used for image acquisition. A TIRF-quality ultra-flat

501 quadruple beam splitter (ZT405/488/561/647rpc; Chroma Technology) for distortion-free

502 reflection of lasers and QUAD emission filter (ZET405/488/561/640m; Chroma) were used.

503 Transfected neurons were identified based on their GFP transfection using excitation with a

504 491-nm laser. For sptPALM, Fyn-mEos2 was photoactivated with low-levels 405-nm laser

505 excitation (100 mW Vortran Laser Technology, 1-3% of initial laser power). Photoactivated

22

506   Fyn-mEos2 molecules were subsequently photoconverted using 561-nm laser (150 mW Cobolt

507   Jive, 70% of initial laser power).

508

509   **Data analysis**

510   Tracking of single molecules of Fyn-mEos2 was performed in accordance with previous

511   publications (Nair et al., 2013). Wavelet-based segmentation was used to detect single

512   localizations of Fyn-mEos2. Following this, tracks of Fyn-mEos2 were computed using

513   simulated annealing-based tracking algorithm implemented in PALM-Tracer, a software that

514   operates in MetaMorph (Molecular Devices). Tracks lasting a minimum of eight frames were

515   reconstructed and used to calculate the mean-square displacement (MSD) of Fyn-mEos2 using

516   the equation MSD (t) = a + 4Dt, where D is the diffusion coefficient, a=y intercept and t=time.

517   Trajectories with $Log_{10}[D] > -1.6$ were considered to be mobile, allowing us to plot a frequency

518   distribution histogram of $Log_{10}[D]$ and calculate the relative portion of mobile to immobile

519   Fyn-mEos2 molecules (Bademosi et al., 2017; Constals et al., 2015). Fyn nanoclustering was

520   quantified and visualised from sptPALM data using custom Python scripting based around the

521   Density-Based Spatial Clustering of Applications with Noise (DBSCAN) functionality of the

522   Python SciKit-Learn module (scikit-learn.org). Spatial centroids for each trajectory (with a

523   minimum of eight steps) in a region of interest were clustered using DBSCAN with empirically

524   determined "Goldilocks" values of ε = 0.1 μm (radius around each centroid to check for other

525   centroids) and MinPts = 3 (minimum number of centroids within this radius to be considered

526   a cluster). For each DBSCAN cluster, a convex hull of all the localizations comprising the

527   clustered trajectories was used to determine the cluster area.

528

529   **Statistics**

530   The D'Agostino and Pearson test was used to test for normality. For statistical analysis between

531   two groups, a Student's t-test was used. For multiple comparisons, a one-way ANOVA was

532   used with the Tukey's test for corrections for multiple comparisons. Statistical comparisons

533   were performed on a per-cell basis (Fig 2-3, 5-7) and a per-cluster basis (Fig 4). The neurons

534   analysed for each experiment were derived from a dissection of a minimum of five embryos.

535   Unless otherwise stated, values are represented as the mean ± SEM. The tests used are indicated

536   in the respective figure legends. For all statistical comparisons, p<0.05 was considered to be

537   statistically significant. The tests used are indicated in the respective figure legends. Data were

538   considered significant at p < 0.05. Statistical tests were performed, and figures were made using

539   GraphPad Prism 7. A summary of statistical analyses is provided in Supplementary table 1.

540

541

542   **Figure legends**

543

544   **Figure 1.** Single molecule imaging photoactivated localization microscopy (sptPALM) of Fyn-

545   mEos2 co-transfected with GFP in secondary dendritic branches and spines of hippocampal

546   neurons (DIV19-22). **A.** Illustration showing the structure and conformation of Fyn-mEos2.

547   Key epitopes found in the SH1 domain and C terminus of Fyn are highlighted. **(i)** Secondary

548   structure and domain alignment of Fyn. **(iii)** Tertiary structure of Fyn, closed conformation **(iii)**

549   Tertiary structure of Fyn, open conformation. mEos2 is conjugated to the C-terminus of Fyn.

550   **B.** Panels depict GFP epifluorescence and intensity, diffusion coefficient and tracking maps of

551   Fyn-mEos2 (note: hotter colours within diffusion coefficient maps designate regions of low

552   mobility). Scale bar = 4 μm (dendrites) and 1 μm (spines). **C.** Frequency distribution (%) of

553   postsynaptic Fyn-mEos2 mobility, $Log_{10}[D](\mu m^2 s^{-1})$, where [D] is the diffusion coefficient. **(i-**

554   **iii)** Examples of frequency of diffusion of Fyn-mEos2 from individual neurons. **(iv)** Averaged

555   frequency distribution. Mobile:immobile fraction threshold is set at -1.6 $\mu m^2 s^{-1}$.

556

557   **Figure 2.** Inhibition of the catalytic (SH1) domain does not impact the mobility of Fyn-mEos2

558   **A.** Illustration depicting K299M and Y420F mutants in closed conformation of Fyn. **B.**

559   Intensity and diffusion coefficient maps for Fyn-mEos2 (wild-type, K299M, Y420F). **C.**

560   Mobility of Fyn-mEos2 in dendrites. **D.** Mobility of Fyn-mEos2 in spines. **(i)** Frequency

561   distribution of Log_{10} [D]($\mu m^2 s^{-1}$) where [D] is the diffusion coefficient, together with the

562   immobile fraction (%). **(ii)** Mean square displacement (MSD) of Fyn-mEos2 over time (0.14

563   sec) with corresponding area under curve (AUC) [($\mu m^2 s$) × 100]. Error bars are standard errors

564   of the mean (SEM). Mean ± SEM values were obtained for neurons transfected with Fyn-WT-

565   mEos2 (n = 14), Fyn-K299M-mEos2 (n=12) and Fyn-Y420F-mEos2 (n=8). Statistical

566   comparisons were performed using a Student's t test.

567

568   **Figure 2 – Figure supplement 1.** Pharmacological inhibition of the catalytic activity of Fyn

569   with pyrazolopyrimidine 2 (PP2) does not impact its mobility. **A.** Illustration depicting the

570   pharmacological inhibition of Fyn in closed and open conformation with PP2. **B.** Mobility of

571   Fyn-mEos2. **(i)** Frequency distribution of Log_{10}[D]($\mu m^2 s^{-1}$) where [D] is the diffusion

572   coefficient **(ii)** the immobile fraction (%). Error bars are standard errors of the mean (SEM).

573   Mean ± SEM values were obtained for neurons transfected with Fyn-WT-mEos2 treated with

574   PP3 (n=9) and PP2 (n=11). Statistical comparisons were performed using the Student's t test.

575

576   **Figure 3.** Phosphorylation of the Y531 epitope controls the lateral entrapment of Fyn-mEos2

577   in the dendrites and spines of hippocampal neurons. **A.** Illustration depicting **(i)** the Y531

578   epitope in the closed conformation of Fyn and **(ii)** the Y531F mutation triggering an open

579 conformation of Fyn. **B.** Intensity and diffusion coefficient maps of Fyn-mEos2 localisations

580 within spines of hippocampal dendrites. Scale bar = 1 μm. **C.** Mobility of Fyn-mEos2 in

581 hippocampal dendrites. **(i)** Frequency distribution of diffusion coefficient values together with

582 immobile fraction (%). **(ii)** Mean square displacement (MSD) of Fyn-mEos2 over time (0.14

583 s) with the corresponding area under curve (AUC) [(μm^2 s) × 100]. **D.** Mobility of Fyn-mEos2

584 in hippocampal spines. **(i)** Frequency distribution of diffusion coefficient values together with

585 immobile fraction (%). **(ii)** Mean square displacement (MSD) of Fyn-mEos2 over time (0.14

586 s) with the corresponding area under curve (AUC) [(μm^2 s) × 100]. Error bars are standard

587 errors of the mean (SEM). Mean ± SEM values were obtained for neurons transfected with

588 Fyn-WT-mEos2 (n = 8), Fyn-Y531F-mEos2 (n=14) and Y531F-K299M-mEos2 (n=9).

589 Statistical comparisons were performed using a one-way ANOVA and Tukey's test for

590 comparisons between groups.

591

592 **Figure 4.** Nanoclustering and step length distribution of Fyn-mEos2 in the dendrites of

593 hippocampal neurons revealed by density-based clustering analysis (DBSCAN). The Y531F

594 mutation, which induces entry of Fyn into an open, active conformation, increases the density

595 and decreases the size of Fyn-mEos2 nanoclusters. **A.** Frequency distribution of step lengths

596 (μm) of Fyn-mEos2. No change in the frequency distribution of steps taken was observed

597 between Fyn-WT-mEos2 and Fyn-Y531F-mEos2. **B.** Spatial distribution of Fyn-mEos2

598 nanoclusters in the dendrites and spines. Scale bar = 1 μm. **C. (i)** Mean square displacement

599 (MSD) (μm^2) over time (200 ms) plotted for clustered and unclustered populations of Fyn-

600 mEos2. **(ii)** Average cluster MSD AUC (μm^{2}s) for Fyn-WT-mEos2 and Fyn-Y531F-mEos2.

601 **D.** Nanocluster dynamics of Fyn-WT-mEos2 and Fyn-Y531F-mEos2. **(i)** Cluster membership

602 (trajectory number). **(ii)** Cluster density (trajectories/μm^2). **(iii)** Cluster area (μm^2).

603 Nanoclusters were significantly denser for Fyn-Y531F-mEos2 compared to Fyn-WT-mEos2.

604   Error bars are standard errors of the mean (SEM). Mean ± SEM values were obtained from n

605   = 823 nanoclusters (Fyn-WT-mEos2) and n=698 (Fyn-Y531F-mEos2) from 5 neurons.

606   Statistical comparisons were performed using a Student's t test.

607

608   **Figure 5.** Deletion of the SH3 domain promotes the lateral trapping of Fyn-mEos2. **A.**

609   Schematic showing deletion of the SH3 domain (ΔSH3). **B.** Intensity and diffusion coefficient

610   maps of Fyn-mEos2 (WT, ΔSH3) in hippocampal neurons. Scale bar = 1 μm. **C**. Frequency

611   distribution of diffusion coefficient values, where [D]=diffusion coefficient, together with the

612   immobile fraction (%). **D.** Mean square displacement (MSD) over time (0.14 s) with

613   corresponding area under curve (AUC) [(μm^2 s) × 100] of Fyn-mEos2 (WT, ΔSH3) in

614   hippocampal dendrites (DIV18-22). Error bars are standard errors of the mean (SEM). Mean ±

615   SEM values were obtained from neurons transfected with Fyn-WT-mEos2 (n=19) and Fyn-

616   ΔSH3-mEos2 (n = 13). Statistical comparisons were performed using a one-way ANOVA and

617   Tukey's test for comparisons between groups.

618

619   **Figure 6.** Binding of anti-Fyn intrabodies to the SH3 domain decreases the mobility of Fyn-

620   GFP in HEK293T cells. **A.** Schematic depicting binding of anti-Fyn-mEos2 intrabodies to the

621   SH3 domain and anti-GFP-mEos2 intrabodies to Fyn-GFP. **B.** Anti-GFP-mEos2 and anti-Fyn

622   (SH3)-mEos2 tracking of Fyn-GFP in HEK293T cells. Scale bar = 4 μm for epifluorescence

623   and 1 μm for track panels. **C. (i)** Frequency distribution of diffusion coefficient values together

624   with immobile fraction (%) and **(ii)** MSD over time (0.14 sec) with AUC [(μm^2 s) × 100] of

625   Fyn-mEos2, anti-GFP-mEos2/Fyn-GFP or anti-SH3-mEos2/Fyn-GFP in HEK293T cells.

626   Error bars are standard errors of the mean (SEM). Mean ± SEM values were obtained from

627   HEK293T cells transfected with Fyn-mEos2 (n=11), Fyn-GFP treated with anti-GFP-mEos2

628   (n=7) or anti-Fyn-mEos2 (n=7). Statistical comparisons were performed using a one-way

629   ANOVA and Tukey's test.

630

631   **Figure 7.** Overexpression of tau (WT, P301L) decreases the mobility and increases activity of

632   Fyn. **A.** Intensity map of Fyn-mEos2 co-expressed with GFP, tau-WT-GFP and tau-P301L-

633   GFP in the spines of mouse hippocampal neurons (DIV19-22). Scale bar = 1 µm. **B**. Frequency

634   distribution (%) of Log_{10} [D] of Fyn-mEos2 with immobile fraction (%). **C**. Mean square

635   displacement (MSD) of Fyn-mEos2 over time (0.14 sec) and area under curve (AUC) [(µm^2 s)

636   × 100]. **D.** Increased phosphorylation at the Y16 epitope in the presence of tau P301L. Western

637   blot of Fyn in protein extracts derived from HEK293 cells co-transfected with Fyn-WT-mEos2

638   and GFP, tau-WT-GFP or tau-P301L-GFP. Fyn-Y420F-mEos2 was also co-transfected with

639   GFP as a control. Activity of Fyn determined by quantifying proportion of active Fyn (anti-

640   Y416) relative to total Fyn, normalised to GAPDH. Co-expression of tau-P301L increased the

641   proportion of active Fyn. Error bars are standard errors of the mean (SEM). Mean ± SEM

642   values were obtained from neurons transfected with Fyn-mEos2+GFP (n = 12), Fyn-

643   mEos2+tau-WT-GFP (n=4) or Fyn-mEos2+tau-P301L-GFP (n=15), and HEK293 protein

644   lysates (n=3 for each group). Statistical comparisons between tau-transfections (A-C) were

645   performed using a one-way ANOVA and Tukey's test for multiple comparisons. A Student's

646   t test was performed for statistical comparisons of Y16 phosphorylation (D).

647

648   **Figure 8.** Model for the lateral entrapment of Fyn, mediated by entry into an open

649   conformation. Tau P301L (brown) binds to the SH3 domain (green) of Fyn and displaces the

650   interaction of SH3 with the linker region (red), which stabilises the open conformation of Fyn.

651   The open conformation of Fyn bound to tau P301L exposes the SH2 domain (blue) of Fyn to

652   interact with additional binding proteins, and positions tau P301L N-termini in close proximity

653 with Fyn's catalytic domain. This extended conformation also causes the lateral entrapment of

654 Fyn.

655

Article and author information

657

Authors contribution

659 R.M.M. and F.A.M. were involved in conceptualisation of the project, design and supervision

660 of the research. R.M.M. and C.S. performed super-resolution experiments. C.S. and R.M.M.

661 analysed the data. T.W. contributed with analytic tools and analysis of the data. R.S.G. created

662 specific plasmids. C.S., R.M.M., and F.A.M. wrote the paper. C.S., R.M.M, F.A.M and J.G.

663 reviewed and edited the manuscript. F.A.M and J.G acquired required funding.

664

Conflict of interest

666 The authors declare no competing financial interests to disclose.

667

685

686 **References**

687

688 Amaya, J., Ryan, V. H., & Fawzi, N. L. (2018, Dec 21). The SH3 domain of Fyn kinase

689   interacts with and induces liquid-liquid phase separation of the low-complexity domain

690   of hnRNPA2. *J Biol Chem, 293*(51), 19522-19531.

691   https://doi.org/10.1074/jbc.RA118.005120

692

693 Bademosi, A. T., Lauwers, E., Padmanabhan, P., Odierna, L., Chai, Y. J., Papadopulos, A.,

694   Goodhill, G. J., Verstreken, P., van Swinderen, B., & Meunier, F. A. (2017, Jan 3). In

695   vivo single-molecule imaging of syntaxin1A reveals polyphosphoinositide- and

696   activity-dependent trapping in presynaptic nanoclusters. *Nat Commun, 8*, 13660.

697   https://doi.org/10.1038/ncomms13660

698

699 Bain, J., McLauchlan, H., Elliott, M., & Cohen, P. (2003, Apr 1). The specificities of protein

700   kinase inhibitors: an update. *Biochem J, 371*(Pt 1), 199-204.

701   https://doi.org/10.1042/BJ20021535

702

703 Bhaskar, K., Hobbs, G. A., Yen, S. H., & Lee, G. (2010, Oct). Tyrosine phosphorylation of tau

704   accompanies disease progression in transgenic mouse models of tauopathy.

705   *Neuropathol Appl Neurobiol, 36*(6), 462-477. https://doi.org/10.1111/j.1365-

706   2990.2010.01103.x

707

708 Bhaskar, K., Yen, S. H., & Lee, G. (2005, Oct 21). Disease-related modifications in tau affect

709   the interaction between Fyn and Tau. *J Biol Chem, 280*(42), 35119-35125.

710   https://doi.org/10.1074/jbc.M505895200

711

712   Blazquez-Llorca, L., Garcia-Marin, V., Merino-Serrais, P., Avila, J., & DeFelipe, J. (2011).

713   Abnormal tau phosphorylation in the thorny excrescences of CA3 hippocampal neurons

714   in patients with Alzheimer's disease. *J Alzheimers Dis, 26*(4), 683-698.

715   https://doi.org/10.3233/JAD-2011-110659

716

717   Briggs, S. D., & Smithgall, T. E. (1999, Sep 10). SH2-kinase linker mutations release Hck

718   tyrosine kinase and transforming activities in Rat-2 fibroblasts. *J Biol Chem, 274*(37),

719   26579-26583. https://doi.org/10.1074/jbc.274.37.26579

720

721   Brigidi, G. S., Santyr, B., Shimell, J., Jovellar, B., & Bamji, S. X. (2015, Sep 3). Activity-

722   regulated trafficking of the palmitoyl-acyl transferase DHHC5. *Nat Commun, 6*, 8200.

723   https://doi.org/10.1038/ncomms9200

724

725   Briner, A., Gotz, J., & Polanco, J. C. (2020, Aug 18). Fyn Kinase Controls Tau Aggregation

726   In Vivo. *Cell Rep, 32*(7), 108045. https://doi.org/10.1016/j.celrep.2020.108045

727

728   Byrne, M. J., Waxham, M. N., & Kubota, Y. (2011, Aug). The impacts of geometry and binding

729   on CaMKII diffusion and retention in dendritic spines. *J Comput Neurosci, 31*(1), 1-

730   12. https://doi.org/10.1007/s10827-010-0293-9

731

732   Cabrales Fontela, Y., Kadavath, H., Biernat, J., Riedel, D., Mandelkow, E., & Zweckstetter,

733   M. (2017, Dec 7). Multivalent cross-linking of actin filaments and microtubules

734   through the microtubule-associated protein Tau. *Nat Commun, 8*(1), 1981.

735   https://doi.org/10.1038/s41467-017-02230-8

736

737 Chai, Y. J., Sierecki, E., Tomatis, V. M., Gormal, R. S., Giles, N., Morrow, I. C., Xia, D., Gotz,

738   J., Parton, R. G., Collins, B. M., Gambin, Y., & Meunier, F. A. (2016, Sep 12). Munc18-

739   1 is a molecular chaperone for alpha-synuclein, controlling its self-replicating

740   aggregation. *J Cell Biol, 214*(6), 705-718. https://doi.org/10.1083/jcb.201512016

741

742 Chin, J., Palop, J. J., Puolivali, J., Massaro, C., Bien-Ly, N., Gerstein, H., Scearce-Levie, K.,

743   Masliah, E., & Mucke, L. (2005, Oct 19). Fyn kinase induces synaptic and cognitive

744   impairments in a transgenic mouse model of Alzheimer's disease. *J Neurosci, 25*(42),

745   9694-9703. https://doi.org/10.1523/JNEUROSCI.2980-05.2005

746

747 Chin, J., Palop, J. J., Yu, G. Q., Kojima, N., Masliah, E., & Mucke, L. (2004, May 12). Fyn

748   kinase modulates synaptotoxicity, but not aberrant sprouting, in human amyloid

749   precursor protein transgenic mice. *J Neurosci, 24*(19), 4692-4697.

750   https://doi.org/10.1523/JNEUROSCI.0277-04.2004

751

752 Cochran, J. N., Diggs, P. V., Nebane, N. M., Rasmussen, L., White, E. L., Bostwick, R.,

753   Maddry, J. A., Suto, M. J., & Roberson, E. D. (2014, Dec). AlphaScreen HTS and live-

754   cell bioluminescence resonance energy transfer (BRET) assays for identification of

755   Tau-Fyn SH3 interaction inhibitors for Alzheimer disease. *J Biomol Screen, 19*(10),

756   1338-1349. https://doi.org/10.1177/1087057114547232

757

758 Constals, A., Penn, A. C., Compans, B., Toulme, E., Phillipat, A., Marais, S., Retailleau, N.,

759   Hafner, A. S., Coussen, F., Hosy, E., & Choquet, D. (2015, Feb 18). Glutamate-induced

760   AMPA receptor desensitization increases their mobility and modulates short-term

761   plasticity through unbinding from Stargazin. *Neuron, 85*(4), 787-803.

762   https://doi.org/10.1016/j.neuron.2015.01.012

763

764   Elie, A., Prezel, E., Guerin, C., Denarier, E., Ramirez-Rios, S., Serre, L., Andrieux, A., Fourest-

765   Lieuvin, A., Blanchoin, L., & Arnal, I. (2015, May 5). Tau co-organizes dynamic

766   microtubule and actin networks. *Sci Rep, 5*, 9964. https://doi.org/10.1038/srep09964

767

768   Engen, J. R., Wales, T. E., Hochrein, J. M., Meyn, M. A., 3rd, Banu Ozkan, S., Bahar, I., &

769   Smithgall, T. E. (2008, Oct). Structure and dynamic regulation of Src-family kinases.

770   *Cell Mol Life Sci, 65*(19), 3058-3073. https://doi.org/10.1007/s00018-008-8122-2

771

772   Frandemiche, M. L., De Seranno, S., Rush, T., Borel, E., Elie, A., Arnal, I., Lante, F., &

773   Buisson, A. (2014, Apr 23). Activity-dependent tau protein translocation to excitatory

774   synapse is disrupted by exposure to amyloid-beta oligomers. *J Neurosci, 34*(17), 6084-

775   6097. https://doi.org/10.1523/JNEUROSCI.4261-13.2014

776

777   Goose, J. E., & Sansom, M. S. (2013, Apr). Reduced lateral mobility of lipids and proteins in

778   crowded membranes. *PLoS Comput Biol, 9*(4), e1003033.

779   https://doi.org/10.1371/journal.pcbi.1003033

780

781   Gotz, J., Chen, F., van Dorpe, J., & Nitsch, R. M. (2001, Aug 24). Formation of neurofibrillary

782   tangles in P301l tau transgenic mice induced by Abeta 42 fibrils. *Science, 293*(5534),

783   1491-1495. https://doi.org/10.1126/science.1062097

784

785   Grant, S. G., O'Dell, T. J., Karl, K. A., Stein, P. L., Soriano, P., & Kandel, E. R. (1992, Dec

786   18). Impaired long-term potentiation, spatial learning, and hippocampal development

787   in fyn mutant mice. *Science, 258*(5090), 1903-1910.

788   https://doi.org/10.1126/science.1361685

789

790   Haass, C., & Mandelkow, E. (2010, Aug 6). Fyn-tau-amyloid: a toxic triad. *Cell, 142*(3), 356-

791   358. https://doi.org/10.1016/j.cell.2010.07.032

792

793   Hanke, J. H., Pollok, B. A., & Changelian, P. S. (1995, Sep). Role of tyrosine kinases in

794   lymphocyte activation: targets for drug intervention. *Inflamm Res, 44*(9), 357-371.

795   https://doi.org/10.1007/BF01797862

796

797   Hoffmann, N. A., Dorostkar, M. M., Blumenstock, S., Goedert, M., & Herms, J. (2013, Dec

798   17). Impaired plasticity of cortical dendritic spines in P301S tau transgenic mice. *Acta*

799   *Neuropathol Commun, 1*, 82. https://doi.org/10.1186/2051-5960-1-82

800

801   Hoover, B. R., Reed, M. N., Su, J., Penrod, R. D., Kotilinek, L. A., Grant, M. K., Pitstick, R.,

802   Carlson, G. A., Lanier, L. M., Yuan, L. L., Ashe, K. H., & Liao, D. (2010, Dec 22).

803   Tau mislocalization to dendritic spines mediates synaptic dysfunction independently of

804   neurodegeneration. *Neuron, 68*(6), 1067-1081.

805   https://doi.org/10.1016/j.neuron.2010.11.030

806

807   Hruska, M., Henderson, N., Le Marchand, S. J., Jafri, H., & Dalva, M. B. (2018, May).

808   Synaptic nanomodules underlie the organization and plasticity of spine synapses. *Nat*

809   *Neurosci, 21*(5), 671-682. https://doi.org/10.1038/s41593-018-0138-9

810

811   Huang, R., Fang, P., Hao, Z., & Kay, B. K. (2016). Directed Evolution of a Highly Specific

812   FN3 Monobody to the SH3 Domain of Human Lyn Tyrosine Kinase. *PLoS One, 11*(1),

813   e0145872. https://doi.org/10.1371/journal.pone.0145872

814

815   Huang, R., Fang, P., & Kay, B. K. (2012, Jun 15). Isolation of monobodies that bind

816   specifically to the SH3 domain of the Fyn tyrosine protein kinase. *N Biotechnol, 29*(5),

817   526-533. https://doi.org/10.1016/j.nbt.2011.11.015

818

819   Huculeci, R., Cilia, E., Lyczek, A., Buts, L., Houben, K., Seeliger, M. A., van Nuland, N., &

820   Lenaerts, T. (2016, Nov 1). Dynamically Coupled Residues within the SH2 Domain of

821   FYN Are Key to Unlocking Its Activity. *Structure, 24*(11), 1947-1959.

822   https://doi.org/10.1016/j.str.2016.08.016

823

824   Irtegun, S., Wood, R. J., Ormsby, A. R., Mulhern, T. D., & Hatters, D. M. (2013). Tyrosine

825   416 is phosphorylated in the closed, repressed conformation of c-Src. *PLoS One, 8*(7),

826   e71035. https://doi.org/10.1371/journal.pone.0071035

827

828   Ittner, L. M., & Gotz, J. (2011, Feb). Amyloid-beta and tau--a toxic pas de deux in Alzheimer's

829   disease. *Nat Rev Neurosci, 12*(2), 65-72. https://doi.org/10.1038/nrn2967

830

831   Ittner, L. M., Ke, Y. D., Delerue, F., Bi, M., Gladbach, A., van Eersel, J., Wolfing, H., Chieng,

832   B. C., Christie, M. J., Napier, I. A., Eckert, A., Staufenbiel, M., Hardeman, E., & Gotz,

833   J. (2010, Aug 6). Dendritic function of tau mediates amyloid-beta toxicity in

834   Alzheimer's   disease   mouse   models.   *Cell,   142*(3),   387-397.

835   https://doi.org/10.1016/j.cell.2010.06.036

836

837   Jin, D. Z., Mao, L. M., & Wang, J. Q. (2017, Jul-Aug). An Essential Role of Fyn in the

838   Modulation of Metabotropic Glutamate Receptor 1 in Neurons. *eNeuro, 4*(4).

839   https://doi.org/10.1523/ENEURO.0096-17.2017

840

841   Joensuu, M., Martinez-Marmol, R., Padmanabhan, P., Glass, N. R., Durisic, N., Pelekanos, M.,

842   Mollazade, M., Balistreri, G., Amor, R., Cooper-White, J. J., Goodhill, G. J., &

843   Meunier, F. A. (2017, Dec). Visualizing endocytic recycling and trafficking in live

844   neurons by subdiffractional tracking of internalized molecules. *Nat Protoc, 12*(12),

845   2590-2622. https://doi.org/10.1038/nprot.2017.116

846

847   Kasula, R., Chai, Y. J., Bademosi, A. T., Harper, C. B., Gormal, R. S., Morrow, I. C., Hosy,

848   E., Collins, B. M., Choquet, D., Papadopulos, A., & Meunier, F. A. (2016, Sep 26). The

849   Munc18-1 domain 3a hinge-loop controls syntaxin-1A nanodomain assembly and

850   engagement with the SNARE complex during secretory vesicle priming. *J Cell Biol,*

851   *214*(7), 847-858. https://doi.org/10.1083/jcb.201508118

852

853   Kaufman, A. C., Salazar, S. V., Haas, L. T., Yang, J., Kostylev, M. A., Jeng, A. T., Robinson,

854   S. A., Gunther, E. C., van Dyck, C. H., Nygaard, H. B., & Strittmatter, S. M. (2015,

855   Jun). Fyn inhibition rescues established memory and synapse loss in Alzheimer mice.

856   *Ann Neurol, 77*(6), 953-971. https://doi.org/10.1002/ana.24394

857

858   Kedia, S., Ramakrishna, P., Netrakanti, P. R., Jose, M., Sibarita, J. B., Nadkarni, S., & Nair,

859   D. (2020, Apr 21). Real-time nanoscale organization of amyloid precursor protein.

860   *Nanoscale, 12*(15), 8200-8215. https://doi.org/10.1039/d0nr00052c

861

862   Kukenshoner, T., Schmit, N. E., Bouda, E., Sha, F., Pojer, F., Koide, A., Seeliger, M., Koide,

863   S., & Hantschel, O. (2017, May 5). Selective Targeting of SH2 Domain-

864   Phosphotyrosine Interactions of Src Family Tyrosine Kinases with Monobodies. *J Mol*

865   *Biol, 429*(9), 1364-1380. https://doi.org/10.1016/j.jmb.2017.03.023

866

867   Lambert, M. P., Barlow, A. K., Chromy, B. A., Edwards, C., Freed, R., Liosatos, M., Morgan,

868   T. E., Rozovsky, I., Trommer, B., Viola, K. L., Wals, P., Zhang, C., Finch, C. E., Krafft,

869   G. A., & Klein, W. L. (1998, May 26). Diffusible, nonfibrillar ligands derived from

870   Abeta1-42 are potent central nervous system neurotoxins. *Proc Natl Acad Sci U S A,*

871   *95*(11), 6448-6453. https://doi.org/10.1073/pnas.95.11.6448

872

873   Larson, M., Sherman, M. A., Amar, F., Nuvolone, M., Schneider, J. A., Bennett, D. A., Aguzzi,

874   A., & Lesne, S. E. (2012, Nov 21). The complex PrP(c)-Fyn couples human oligomeric

875   Abeta with pathological tau changes in Alzheimer's disease. *J Neurosci, 32*(47), 16857-

876   16871a. https://doi.org/10.1523/JNEUROSCI.1858-12.2012

877

878   Lau, D. H., Hogseth, M., Phillips, E. C., O'Neill, M. J., Pooler, A. M., Noble, W., & Hanger,

879   D. P. (2016, May 18). Critical residues involved in tau binding to fyn: implications for

880   tau phosphorylation in Alzheimer's disease. *Acta Neuropathol Commun, 4*(1), 49.

881   https://doi.org/10.1186/s40478-016-0317-4

882

883   Lee, G., Newman, S. T., Gard, D. L., Band, H., & Panchamoorthy, G. (1998, Nov). Tau

884   interacts with src-family non-receptor tyrosine kinases. *J Cell Sci, 111 (Pt 21)*, 3167-

885   3177. https://www.ncbi.nlm.nih.gov/pubmed/9763511

886

887   Lee, G., Thangavel, R., Sharma, V. M., Litersky, J. M., Bhaskar, K., Fang, S. M., Do, L. H.,

888   Andreadis, A., Van Hoesen, G., & Ksiezak-Reding, H. (2004, Mar 3). Phosphorylation

889   of tau by fyn: implications for Alzheimer's disease. *J Neurosci, 24*(9), 2304-2312.

890   https://doi.org/10.1523/JNEUROSCI.4162-03.2004

891

892   Li, C., & Gotz, J. (2017, Nov 2). Somatodendritic accumulation of Tau in Alzheimer's disease

893   is promoted by Fyn-mediated local protein translation. *EMBO J, 36*(21), 3120-3138.

894   https://doi.org/10.15252/embj.201797724

895

896   Li, H., & Lawrence, D. S. (2005, Aug). Acquisition of Fyn-selective SH3 domain ligands via

897   a   combinatorial   library   strategy.   *Chem   Biol,   12*(8),   905-912.

898   https://doi.org/10.1016/j.chembiol.2005.06.007

899

900   Li, T. P., Song, Y., MacGillavry, H. D., Blanpied, T. A., & Raghavachari, S. (2016, Apr 13).

901   Protein Crowding within the Postsynaptic Density Can Impede the Escape of

902   Membrane   Proteins.   *J   Neurosci,   36*(15),   4276-4295.

903   https://doi.org/10.1523/JNEUROSCI.3154-15.2016

904

905   Liu, G., Fiock, K. L., Levites, Y., Golde, T. E., Hefti, M. M., & Lee, G. (2020, Jul 14). Fyn

906   depletion   ameliorates   tau(P301L)-induced   neuropathology. *Acta   Neuropathol

907   Commun, 8*(1), 108. https://doi.org/10.1186/s40478-020-00979-6

908

909   Merino-Serrais, P., Benavides-Piccione, R., Blazquez-Llorca, L., Kastanauskaite, A., Rabano,

910   A., Avila, J., & DeFelipe, J. (2013, Jun). The influence of phospho-tau on dendritic

911   spines of cortical pyramidal neurons in patients with Alzheimer's disease. *Brain, 136*(Pt

912   6), 1913-1928. https://doi.org/10.1093/brain/awt088

913

914   Miller, E. C., Teravskis, P. J., Dummer, B. W., Zhao, X., Huganir, R. L., & Liao, D. (2014,

915   Apr). Tau phosphorylation and tau mislocalization mediate soluble Abeta oligomer-

916   induced AMPA glutamate receptor signaling deficits. *Eur J Neurosci, 39*(7), 1214-

917   1224. https://doi.org/10.1111/ejn.12507

918

919   Miyamoto, T., Stein, L., Thomas, R., Djukic, B., Taneja, P., Knox, J., Vossel, K., & Mucke, L.

920   (2017, May 19). Phosphorylation of tau at Y18, but not tau-fyn binding, is required for

921   tau to modulate NMDA receptor-dependent excitotoxicity in primary neuronal culture.

922   *Mol Neurodegener, 12*(1), 41. https://doi.org/10.1186/s13024-017-0176-x

923

924   Moroco, J. A., Craigo, J. K., Iacob, R. E., Wales, T. E., Engen, J. R., & Smithgall, T. E. (2014).

925   Differential sensitivity of Src-family kinases to activation by SH3 domain

926   displacement. *PLoS One, 9*(8), e105629. https://doi.org/10.1371/journal.pone.0105629

927

928   Morton, C. J., Pugh, D. J., Brown, E. L., Kahmann, J. D., Renzoni, D. A., & Campbell, I. D.

929   (1996, Jun 15). Solution structure and peptide binding of the SH3 domain from human

930   Fyn. *Structure, 4*(6), 705-714. https://doi.org/10.1016/s0969-2126(96)00076-7

931

932   Nair, D., Hosy, E., Petersen, J. D., Constals, A., Giannone, G., Choquet, D., & Sibarita, J. B.

933   (2013, Aug 7). Super-resolution imaging reveals that AMPA receptors inside synapses

934   are dynamically organized in nanodomains regulated by PSD95. *J Neurosci, 33*(32),

935   13204-13224. https://doi.org/10.1523/JNEUROSCI.2381-12.2013

936

937   Nakazawa, T., Komai, S., Tezuka, T., Hisatsune, C., Umemori, H., Semba, K., Mishina, M.,

938   Manabe, T., & Yamamoto, T. (2001, Jan 5). Characterization of Fyn-mediated tyrosine

939   phosphorylation sites on GluR epsilon 2 (NR2B) subunit of the N-methyl-D-aspartate

940   receptor. *J Biol Chem, 276*(1), 693-699. https://doi.org/10.1074/jbc.M008085200

941

942   Neddens, J., Temmel, M., Flunkert, S., Kerschbaumer, B., Hoeller, C., Loeffler, T.,

943   Niederkofler, V., Daum, G., Attems, J., & Hutter-Paier, B. (2018, Jun 29).

944   Phosphorylation of different tau sites during progression of Alzheimer's disease. *Acta*

945   *Neuropathol Commun, 6*(1), 52. https://doi.org/10.1186/s40478-018-0557-6

946

947   Nika, K., Soldani, C., Salek, M., Paster, W., Gray, A., Etzensperger, R., Fugger, L., Polzella,

948   P., Cerundolo, V., Dushek, O., Hofer, T., Viola, A., & Acuto, O. (2010, Jun 25).

949   Constitutively active Lck kinase in T cells drives antigen receptor signal transduction.

950   *Immunity, 32*(6), 766-777. https://doi.org/10.1016/j.immuni.2010.05.011

951

952   Padmanabhan, P., Bademosi, A. T., Kasula, R., Lauwers, E., Verstreken, P., & Meunier, F. A.

953   (2020, Jun 1). Need for speed: Super-resolving the dynamic nanoclustering of syntaxin-

954   1   at   exocytic   fusion   sites.   *Neuropharmacology,   169*,   107554.

955   https://doi.org/10.1016/j.neuropharm.2019.02.036

956

957   Padmanabhan, P., Martinez-Marmol, R., Xia, D., Gotz, J., & Meunier, F. A. (2019, Jun 25).

958   Frontotemporal dementia mutant Tau promotes aberrant Fyn nanoclustering in

959   hippocampal dendritic spines. *Elife, 8*. https://doi.org/10.7554/eLife.45040

960

961   Polanco, J. C., Li, C., Bodea, L. G., Martinez-Marmol, R., Meunier, F. A., & Gotz, J. (2018,

962   Jan). Amyloid-beta and tau complexity - towards improved biomarkers and targeted

963   therapies. *Nat Rev Neurol, 14*(1), 22-39. https://doi.org/10.1038/nrneurol.2017.162

964

965   Rapoport, M., Dawson, H. N., Binder, L. I., Vitek, M. P., & Ferreira, A. (2002, Apr 30). Tau

966   is essential to beta -amyloid-induced neurotoxicity. *Proc Natl Acad Sci U S A, 99*(9),

967   6364-6369. https://doi.org/10.1073/pnas.092136199

968

969   Renner, M., Lacor, P. N., Velasco, P. T., Xu, J., Contractor, A., Klein, W. L., & Triller, A.

970   (2010, Jun 10). Deleterious effects of amyloid beta oligomers acting as an extracellular

971   scaffold for mGluR5. *Neuron, 66*(5), 739-754.

972   https://doi.org/10.1016/j.neuron.2010.04.029

973

974   Reynolds, C. H., Garwood, C. J., Wray, S., Price, C., Kellie, S., Perera, T., Zvelebil, M., Yang,

975   A., Sheppard, P. W., Varndell, I. M., Hanger, D. P., & Anderton, B. H. (2008, Jun 27).

976   Phosphorylation regulates tau interactions with Src homology 3 domains of

977   phosphatidylinositol 3-kinase, phospholipase Cgamma1, Grb2, and Src family kinases.

978   *J Biol Chem, 283*(26), 18177-18186. https://doi.org/10.1074/jbc.M709715200

979

980   Rush, T., Roth, J. R., Thompson, S. J., Aldaher, A. R., Cochran, J. N., & Roberson, E. D. (2020,

981   Feb). A peptide inhibitor of Tau-SH3 interactions ameliorates amyloid-beta toxicity.

982   *Neurobiol Dis, 134*, 104668. https://doi.org/10.1016/j.nbd.2019.104668

983

984   Sato, I., Obata, Y., Kasahara, K., Nakayama, Y., Fukumoto, Y., Yamasaki, T., Yokoyama, K.

985   K., Saito, T., & Yamaguchi, N. (2009, Apr 1). Differential trafficking of Src, Lyn, Yes

986   and Fyn is specified by the state of palmitoylation in the SH4 domain. *J Cell Sci, 122*(Pt

987   7), 965-975. https://doi.org/10.1242/jcs.034843

988

989   Shrivastava, A. N., Aperia, A., Melki, R., & Triller, A. (2017, Jul 5). Physico-Pathologic

990   Mechanisms Involved in Neurodegeneration: Misfolded Protein-Plasma Membrane

991   Interactions. *Neuron, 95*(1), 33-50. https://doi.org/10.1016/j.neuron.2017.05.026

992

993   Sicheri, F., & Kuriyan, J. (1997, Dec). Structures of Src-family tyrosine kinases. *Curr Opin*

994   *Struct Biol, 7*(6), 777-785. https://doi.org/10.1016/s0959-440x(97)80146-7

995

996   Tang, S. J., Fesharaki-Zadeh, A., Takahashi, H., Nies, S. H., Smith, L. M., Luo, A., Chyung,

997   A., Chiasseu, M., & Strittmatter, S. M. (2020, Jul 1). Fyn kinase inhibition reduces

998   protein aggregation, increases synapse density and improves memory in transgenic and

999   traumatic Tauopathy. *Acta Neuropathol Commun, 8*(1), 96.

1000   https://doi.org/10.1186/s40478-020-00976-9

1001

1002   Tezuka, T., Umemori, H., Akiyama, T., Nakanishi, S., & Yamamoto, T. (1999, Jan 19). PSD-

1003   95 promotes Fyn-mediated tyrosine phosphorylation of the N-methyl-D-aspartate

1004   receptor subunit NR2A. *Proc Natl Acad Sci U S A, 96*(2), 435-440.

1005   https://doi.org/10.1073/pnas.96.2.435

1006

1007   Tomatis, V. M., Papadopulos, A., Malintan, N. T., Martin, S., Wallis, T., Gormal, R. S.,

1008   Kendrick-Jones, J., Buss, F., & Meunier, F. A. (2013, Feb 4). Myosin VI small insert

1009   isoform maintains exocytosis by tethering secretory granules to the cortical actin. *J Cell*

1010   *Biol, 200*(3), 301-320. https://doi.org/10.1083/jcb.201204092

1011

1012   Topinka, J. R., & Bredt, D. S. (1998, Jan). N-terminal palmitoylation of PSD-95 regulates

1013   association with cell membranes and interaction with K+ channel Kv1.4. *Neuron,*

1014   *20*(1), 125-134. https://doi.org/10.1016/s0896-6273(00)80440-7

1015

1016   Torreno-Pina, J. A., Manzo, C., Salio, M., Aichinger, M. C., Oddone, A., Lakadamyali, M.,

1017   Shepherd, D., Besra, G. S., Cerundolo, V., & Garcia-Parajo, M. F. (2016, Feb 9). The

1018   actin cytoskeleton modulates the activation of iNKT cells by segregating CD1d

1019   nanoclusters on antigen-presenting cells. *Proc Natl Acad Sci U S A, 113*(6), E772-781.

1020   https://doi.org/10.1073/pnas.1514530113

1021

1022   Twamley, G. M., Kypta, R. M., Hall, B., & Courtneidge, S. A. (1992, Oct). Association of Fyn

1023   with the activated platelet-derived growth factor receptor: requirements for binding and

1024   phosphorylation. *Oncogene, 7*(10), 1893-1901.

1025   https://www.ncbi.nlm.nih.gov/pubmed/1408131

1026

1027   Twamley-Stein, G. M., Pepperkok, R., Ansorge, W., & Courtneidge, S. A. (1993, Aug 15).

1028   The Src family tyrosine kinases are required for platelet-derived growth factor-

1029   mediated signal transduction in NIH 3T3 cells. *Proc Natl Acad Sci U S A, 90*(16), 7696-

1030   7700. https://doi.org/10.1073/pnas.90.16.7696

1031

1032 Um, J. W., Nygaard, H. B., Heiss, J. K., Kostylev, M. A., Stagi, M., Vortmeyer, A.,

1033   Wisniewski, T., Gunther, E. C., & Strittmatter, S. M. (2012, Sep). Alzheimer amyloid-

1034   beta oligomer bound to postsynaptic prion protein activates Fyn to impair neurons. *Nat*

1035   *Neurosci, 15*(9), 1227-1235. https://doi.org/10.1038/nn.3178

1036

1037 Usardi, A., Pooler, A. M., Seereeram, A., Reynolds, C. H., Derkinderen, P., Anderton, B.,

1038   Hanger, D. P., Noble, W., & Williamson, R. (2011, Aug). Tyrosine phosphorylation of

1039   tau regulates its interactions with Fyn SH2 domains, but not SH3 domains, altering the

1040   cellular   localization   of   tau.   *FEBS   J,   278*(16),   2927-2937.

1041   https://doi.org/10.1111/j.1742-4658.2011.08218.x

1042

1043 Wang, X., Chang, C., Wang, D., & Hong, S. (2019, Jul). Systematic profiling of SH3-mediated

1044   Tau-Partner interaction network in Alzheimer's disease by integrating in silico analysis

1045   and   in   vitro   assay.   *J   Mol   Graph   Model,   90*,   265-272.

1046   https://doi.org/10.1016/j.jmgm.2019.05.004

1047

1048 Xia, D., & Gotz, J. (2014). Premature lethality, hyperactivity, and aberrant phosphorylation in

1049   transgenic mice expressing a constitutively active form of Fyn. *Front Mol Neurosci, 7*,

1050   40. https://doi.org/10.3389/fnmol.2014.00040

1051

1052 Xia, D., Li, C., & Gotz, J. (2015, May). Pseudophosphorylation of Tau at distinct epitopes or

1053   the presence of the P301L mutation targets the microtubule-associated protein Tau to

1054   dendritic spines. *Biochim Biophys Acta, 1852*(5), 913-924.

1055   https://doi.org/10.1016/j.bbadis.2014.12.017

1056

1057   Yadav, S. S., & Miller, W. T. (2007, Nov 8). Cooperative activation of Src family kinases by

1058   SH3 and SH2 ligands. *Cancer Lett, 257*(1), 116-123.

1059   https://doi.org/10.1016/j.canlet.2007.07.012

1060

1061   Young, M. A., Gonfloni, S., Superti-Furga, G., Roux, B., & Kuriyan, J. (2001, Apr 6). Dynamic

1062   coupling between the SH2 and SH3 domains of c-Src and Hck underlies their

1063   inactivation by C-terminal tyrosine phosphorylation. *Cell, 105*(1), 115-126.

1064   https://doi.org/10.1016/s0092-8674(01)00301-4

1065

1066   Zhou, L., McInnes, J., Wierda, K., Holt, M., Herrmann, A. G., Jackson, R. J., Wang, Y. C.,

1067   Swerts, J., Beyens, J., Miskiewicz, K., Vilain, S., Dewachter, I., Moechars, D., De

1068   Strooper, B., Spires-Jones, T. L., De Wit, J., & Verstreken, P. (2017, May 11). Tau

1069   association with synaptic vesicles causes presynaptic dysfunction. *Nat Commun, 8*,

1070   15295. https://doi.org/10.1038/ncomms15295

1071

1072   Zhu, X., Kim, J. L., Newcomb, J. R., Rose, P. E., Stover, D. R., Toledo, L. M., Zhao, H., &

1073   Morgenstern, K. A. (1999, Jun 15). Structural analysis of the lymphocyte-specific
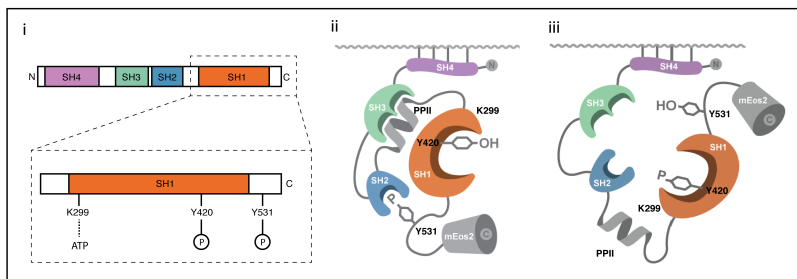
1074   kinase Lck in complex with non-selective and Src family selective kinase inhibitors.

1075   *Structure, 7*(6), 651-661. https://doi.org/10.1016/s0969-2126(99)80086-0

1076

1077

A Fyn kinase structure and conformation

i

ii

iii

B Single particle tracking of Fyn-mEos2

GFP epifluorescence

Fyn-mEos2 intensity

GFP epifluorescence

Fyn-mEos2 intensity

Fyn-mEos2 diffusion coefficient

Fyn-mEos2 trajectories

Fyn-mEos2 diffusion coefficient

Fyn-mEos2 trajectories
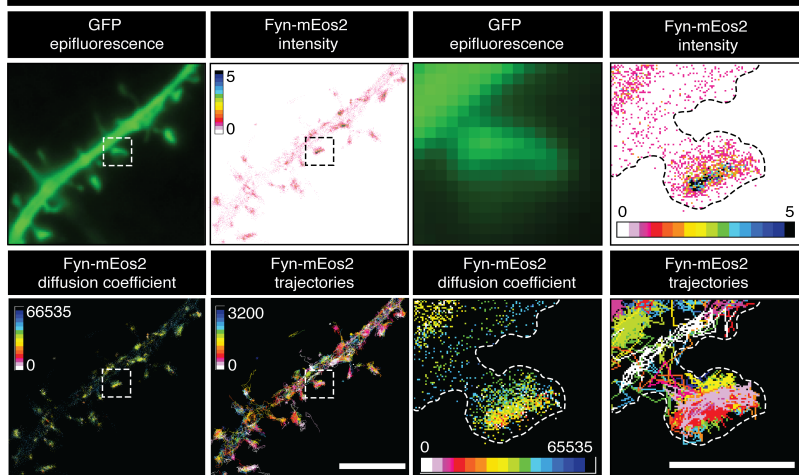
C Fyn-mEos2 postsynaptic mobility (diffusion coefficient)
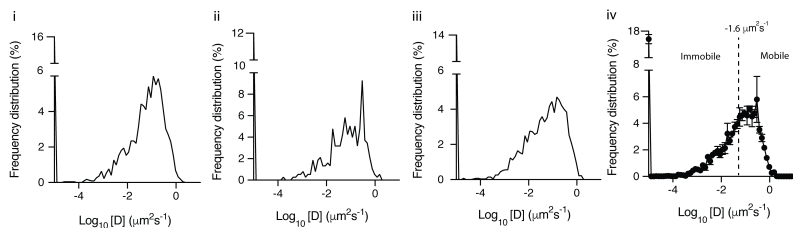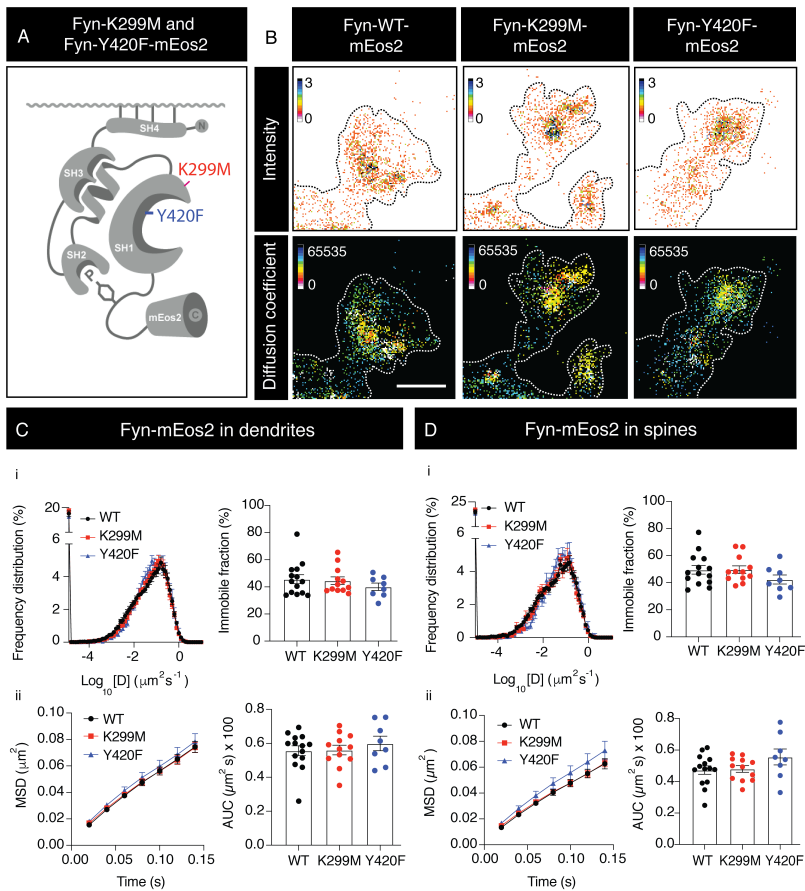
i

ii

iii

iv

Figure 1

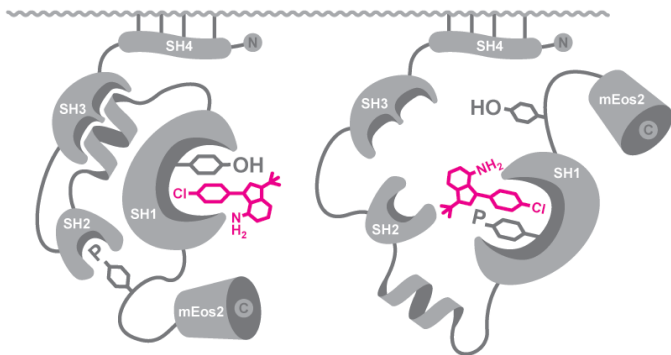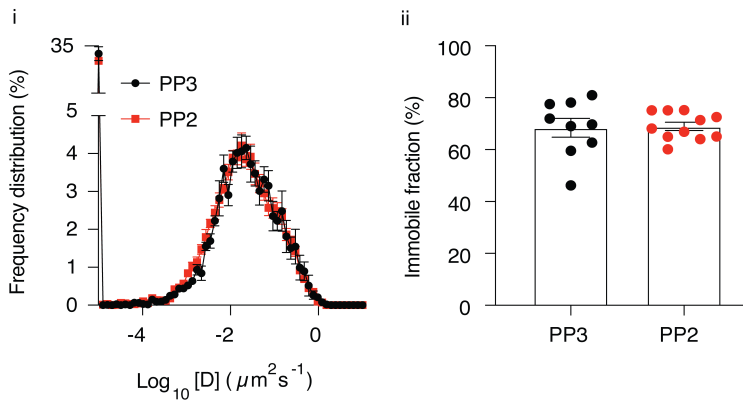Figure 2

A Pharmacological inhibition of Fyn-mEos2 with pyrazolopyramidine 2 (PP2)

B Fyn-mEos2 mobility during PP2 treatment

i

Frequency distribution (%)
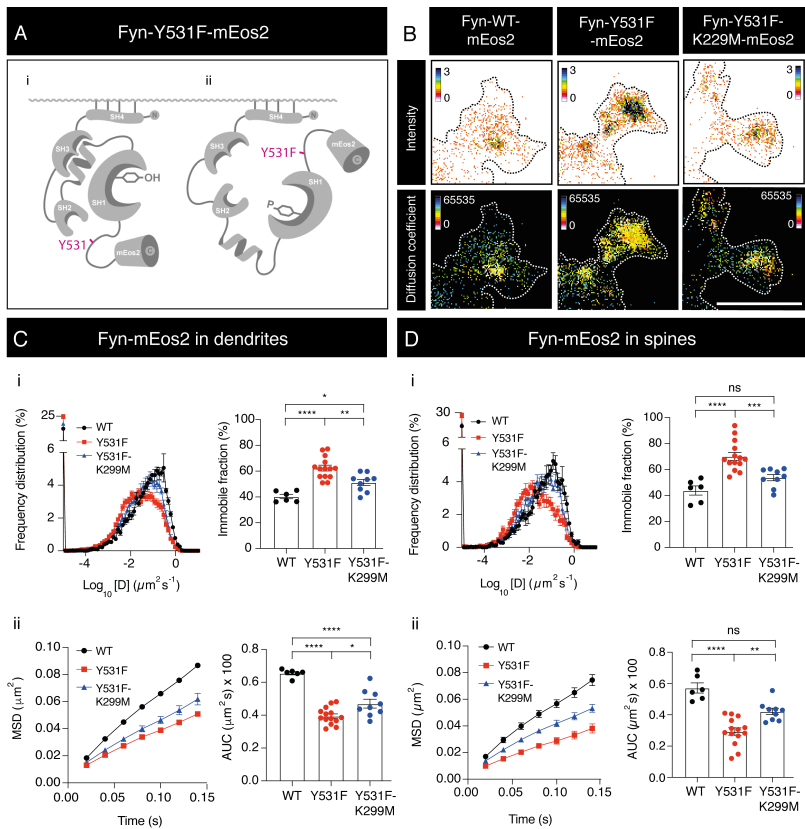
- PP3
- PP2

$\text{Log}_{10}[D]\,(\mu m^2 s^{-1})$

ii

Immobile fraction (%)

PP3 PP2

Supplemental figure 1
(Figure 2)

Figure 3

A — Fyn-Y531F-mEos2

B — Fyn-WT-mEos2 / Fyn-Y531F-mEos2 / Fyn-Y531F-K229M-mEos2

Intensity / Diffusion coefficient

C — Fyn-mEos2 in dendrites

i — Frequency distribution (%) vs Log$_{10}$[D] ($\mu m^2 s^{-1}$); WT, Y531F, Y531F-K299M. Immobile fraction (%): WT, Y531F, Y531F-K299M

ii — MSD (μm^2) vs Time (s); WT, Y531F, Y531F-K299M. AUC ($\mu m^2 s$) × 100: WT, Y531F, Y531F-K299M

D — Fyn-mEos2 in spines

i — Frequency distribution (%) vs Log$_{10}$[D] ($\mu m^2 s^{-1}$); WT, Y531F, Y531F-K299M. Immobile fraction (%): WT, Y531F, Y531F-K299M

ii — MSD (μm^2) vs Time (s); WT, Y531F, Y531F-K299M. AUC ($\mu m^2 s$) × 100: WT, Y531F, Y531F-K299M

A Step length distribution

B Dendritic nanoclustering of Fyn-mEos2

C Mobility of nanoclustered Fyn-mEos2

D Nanoclustering dynamics of Fyn-mEos2 (WT, Y531F)

Figure 4

A

Fyn-WT
N SH4 | SH3 | SH2 | SH1 C

Fyn-ΔSH3
N SH4 | SH2 | SH1 C

B

| Intensity | Diffusion coefficient |

Fyn-WT-mEos2

Fyn-ΔSH3-mEos2

C

WT
ΔSH3

Frequency distribution (%)

$Log_{10}[D](\mu m^2 s^{-1})$

***

Immobile fraction (%)

WT ΔSH3

D

WT
ΔSH3

MSD (μm^2)

Time (s)

***

AUC $(\mu m^2 s) \times 100$

WT ΔSH3

Figure 5

A

B Epifluorescence   Tracks

Anti-GFP-mEos2

Anti-Fyn-mEos2

C

i

Fyn-mEos2
Fyn-GFP + NB-anti-GFP
Fyn-GFP + NB-anti-Fyn

Frequency distribution (%)

Log$_{10}$ [D] ($\mu m^2 s^{-1}$)

% Immobile

Fyn-mEos2   Anti-GFP   Anti-Fyn
Fyn-GFP

ii

Fyn-mEos2
Fyn-GFP + NB-anti-GFP
Fyn-GFP +NB-anti-Fyn

MSD (μm^2)

Time (s)

ns
ns   *

AUC ($\mu m^2 s$) x 100
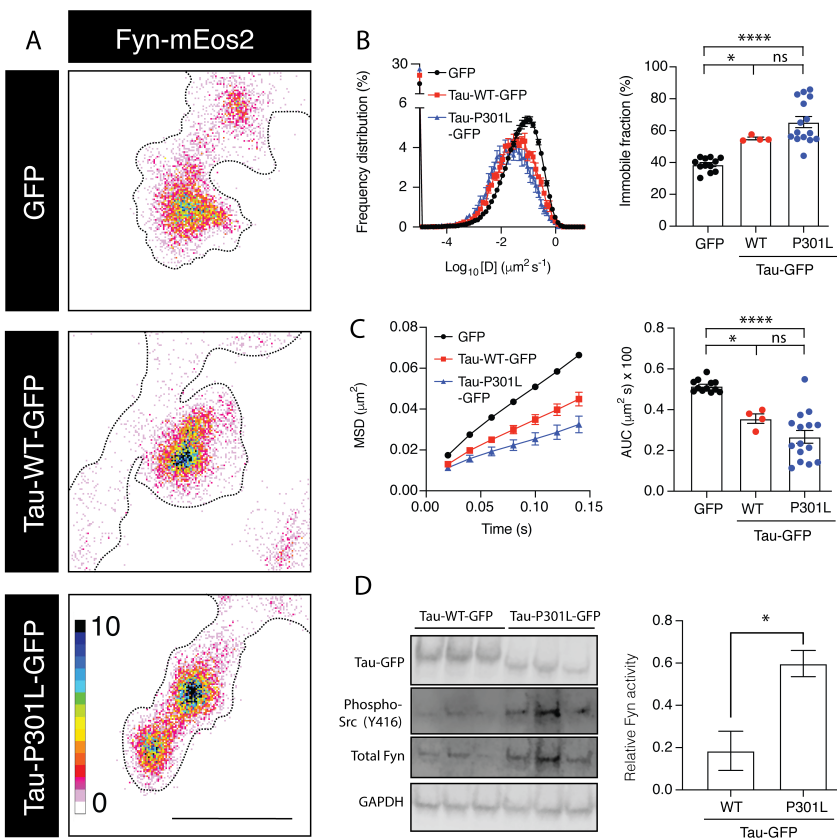
Fyn-mEos2   Anti-GFP   Anti-Fyn
Fyn-GFP

Figure 6

Figure 7

Hypothetical model: tau P301L controls the conformation and mobility state of Fyn kinase

Tau P301L

Closed conformation, Brownian motion

Open conformation, confined

Figure 8